



**HAL**  
open science

## Laboratory measurements and calculations of line shape parameters of the H<sub>2</sub>O-CO<sub>2</sub> collision system

L. Regalia, Julien Cousin, R.R. Gamache, B. Vispoel, S. Robert, X. Thomas

### ► To cite this version:

L. Regalia, Julien Cousin, R.R. Gamache, B. Vispoel, S. Robert, et al.. Laboratory measurements and calculations of line shape parameters of the H<sub>2</sub>O-CO<sub>2</sub> collision system. *Journal of Quantitative Spectroscopy and Radiative Transfer*, 2019, 10.1016/j.jqsrt.2019.04.012 . hal-02104684

**HAL Id: hal-02104684**

**<https://hal.univ-reims.fr/hal-02104684>**

Submitted on 22 Oct 2021

**HAL** is a multi-disciplinary open access archive for the deposit and dissemination of scientific research documents, whether they are published or not. The documents may come from teaching and research institutions in France or abroad, or from public or private research centers.

L'archive ouverte pluridisciplinaire **HAL**, est destinée au dépôt et à la diffusion de documents scientifiques de niveau recherche, publiés ou non, émanant des établissements d'enseignement et de recherche français ou étrangers, des laboratoires publics ou privés.



Distributed under a Creative Commons Attribution - NonCommercial 4.0 International License

LABORATORY MEASUREMENTS AND CALCULATIONS OF LINE SHAPE  
PARAMETERS OF THE H<sub>2</sub>O-CO<sub>2</sub> COLLISION SYSTEM

L. REGALIA<sup>1,\*</sup>, E. COUSIN<sup>1</sup>, R.R. GAMACHE<sup>2</sup>, B. VISPOEL<sup>2</sup>, S. ROBERT<sup>3</sup>, X.  
THOMAS<sup>1</sup>

<sup>1</sup> Groupe de Spectrométrie Moléculaire et Atmosphérique, UMR CNRS 7331, UFR Sciences Exactes et Naturelles, Moulin de la Housse, BP 1039 – 51687 Reims Cedex 2, France

<sup>2</sup> Department of Environmental, Earth, and Atmospheric Sciences, University of Massachusetts Lowell, 1 University Avenue, Lowell, MA 01854, USA

<sup>3</sup> Planetary Aeronomy, Royal Belgian Institute for Space Aeronomy, 3 Avenue Circulaire, 1180 Brussels, Belgium

**Keywords:** high resolution infrared spectroscopy; line shape parameters; Modified Complex Robert-Bonamy calculations, planetary atmospheres; water vapor-carbon dioxide

Number of Pages: 22

Number of Figures: 7

Number of Tables: 4

---

\* Corresponding author. Tel.: +33 326913319, Fax: +33 326913147

E-mail address: [laurence.regalia@univ-reims.fr](mailto:laurence.regalia@univ-reims.fr) (Laurence Régalia)

## *Abstract*

For decades, the remote sensing measurements have been made in planetary atmospheres in the Solar System and beyond. As the performance of the space instruments improves, the atmospheric science community is more and more in need of accurate spectroscopic data. The current databases offer some parameters for non-Earth atmospheres but are far from complete for all situations. For example, measured H<sub>2</sub>O line parameters in CO<sub>2</sub>-rich atmospheres such as Mars and Venus are missing while they are of prime importance to learn about the evolution of the atmospheres. New Fourier Transform Spectrometer spectra were recorded respectively around 2.7 and 6 μm, using a Connes' type FT spectrometer built in Reims. The spectra were analysed using a multispectrum fitting procedure to obtain the line-shape parameters of H<sub>2</sub>O broadened by CO<sub>2</sub>. Modified Complex Robert-Bonamy calculations of the half-width, line shift, and their temperature dependence were made in the spectral region from 1300 to 5000 cm<sup>-1</sup>. The measurements and calculations are presented and compared with data available in the literature.

## Introduction

Water is a key molecule in the search for life on other planets. The origins of water on Earth are not yet well understood. In order to gain insights into this topic, the Solar system must be considered as a whole and the water contents of the different planetary and cometary bodies characterized. This study includes the understanding of the water cycle, the determination of the volume mixing ratio and the distribution with altitude of the different isotopologues of water. In particular, the ratio of deuterium to hydrogen (D/H) is a key diagnostic to characterizing the Solar system's evolution.

Several space instruments have flown or are flying around Mars and Venus. While these planets are our closest neighbors, they have a very different atmospheric structure and composition. Nadir viewing, provided that the spectral resolution and the SNR technique are adequate, and solar occultation viewing allow probing an atmosphere layer by layer to give vertical profile information. The solar occultation technique has the advantage of extremely localized sensitivity to the true atmospheric state (i.e. measured by Averaging Kernels), highly peaked on the impact tangent height. These profiles allow isotopic ratios, such as D/H, to be studied. Considering Mars, the ratio is an important evolutionary tracer for the atmosphere, surface, and their interactions in the climate system. The isotopic ratios are very useful because they are not as affected by modification related to the chemistry occurring in Mars' atmosphere as elemental abundances are [1]. Investigations of the D/H ratio with altitude has led to interesting results [2-7]. Studying the spatial distribution of the D/H ratios can also generate interesting data. Villanueva *et al.* [8] used these 2D maps to study strong water isotopic anomalies in the Martian atmosphere; Good *et al.* [9] looked at D/H isotope ratios in the global hydrologic cycle; and Yang *et al.* [10] modeled the D/H ratio of water in the solar nebula during its formation and evolution. These results could be refined if better line parameters were used, especially H<sub>2</sub>O broadened by CO<sub>2</sub> line shape parameters. The

current parameters used by the planetary community rely on empirical adaptation of other line lists or on scaling other broadening species data. In this study, we use our laboratory set-up and multispectrum procedure to provide measured line shape parameters and make state-of-the-art Modified Complex Robert-Bonamy (MCRB) calculations of the half-width, line shift, and their temperature dependence for the H<sub>2</sub>O-CO<sub>2</sub> collision system.

Two spectral ranges of interest were identified around 2.7 and 6 microns and spectra recorded. The 6 micron band was analyzed previously by Brown et al. [11] in 2007, while the 2.7 microns band was the target of a similar study, here in Reims, some twenty years ago [12]. The spectrometer in Reims now has a better signal to noise ratio (~1000) than previously [12] and the software developed to analyse the spectra in a multispectrum procedure [13] allows the retrieval of more consistent line shape parameters. For the deuterated species of water, HDO, measurements were made on transitions in the  $\nu_2$ ,  $\nu_1$ , and  $\nu_3$  bands [14-16] and MCRB calculations were made for the rotation,  $\nu_2$ ,  $\nu_1$ , and  $\nu_3$  bands [14-17]. In the present study, the newly measured spectra were analyzed in order to determine accurate line shape parameters of H<sub>2</sub>O broadened by CO<sub>2</sub>. We compared our measured results to the data available in the literature and with the MCRB calculations described below.

Section 1 describes the experimental conditions of the measured spectra and explains the line parameters retrieval procedure. Section 2 presents the theory and the calculations made. Finally, we will present our line shape measurements and calculations and compare them with literature values.

## 1. Experimental conditions:

### 1.1 Spectra recording

Sixteen spectra were measured at room temperature with the Connes' type Fourier Transform Spectrometer (FTS) [18-20] built in the Group of Molecular and Atmospheric Spectrometry laboratory (GSMA) in Reims, France. This instrument had a 3-meter maximum path difference allowing a non-apodized resolution of  $0.0017\text{ cm}^{-1}$ . Table 1 summarizes the recording conditions of the spectra in the two studied spectral regions. In the  $2.7\text{ }\mu\text{m}$  region, all spectra were recorded with the following optical setup: a  $\text{CaF}_2$  beam splitter, some lenses and  $\text{BaF}_2$  windows and two InSb detectors, while in the  $6\text{ }\mu\text{m}$  region we used two HgCdTe detectors. We always checked in spectral regions near  $10\text{ }\mu\text{m}$  if the sample or the window emission could perturb the study but in the stated situation, we didn't observe anything. In addition to this, in the  $6\text{ }\mu\text{m}$  spectral region to eliminate some waves on the 100 % of transmission of the spectra due to optical windows in the optical path, we had to divide by a spectrum recorded with an empty cell. We used two different optical spectral filters to select the recording spectral regions, the transmission windows are  $1350 - 2300\text{ cm}^{-1}$  and  $3060 - 4370\text{ cm}^{-1}$  respectively for the  $6\text{ }\mu\text{m}$  and  $2.7\text{ }\mu\text{m}$  spectral region. During the experiment, the absorption path was maintained under vacuum and the pressure and the temperature were continuously monitored. Two absorption cells were used: a single-path cell with an optical path length of 13 cm and a 1-meter White cell [21] to achieve absorption path lengths of 4 and 8 meters. As shown in Table 1, for all spectra, the partial pressure of water vapor was kept very low in order to neglect as much as possible the influence of the self-broadening due to the  $\text{H}_2\text{O}$  pressure in the determination of the line-shape parameters. In addition to the spectra listed in Table 1, we recorded a spectrum for each length of the cell, with only a low  $\text{H}_2\text{O}$  pressure (1 Torr). These spectra allowed us to check the instrumental line shape and were used to calibrate the wavenumber scale of the spectra described in Table 1. For the spectral

calibration, the line positions given in Loos et al. [22] were used as reference. This calibration is not crucial, as the multispectrum procedure allows discrimination of the different shifts for a given recording cell. Indeed, as the parameters are fitted simultaneously on several spectra in different experimental conditions, the shift due to the optical set-up is a parameter with the same value for all spectra, while the shift due to the pressure of the gas (absorbing or foreign) is depending on the studied spectrum.

The carbon dioxide buffer gas was supplied by Air Liquide company with a stated purity of 99.9999%. The pressure was measured with an uncertainty less than 0.3% using two MKS Baratron manometers with 10 and 1000 Torr full scale. The temperature was measured with a platinum probe with an uncertainty less than 0.5 K.

### **Table 1**

The Figure 1 shows an example of the record spectra in the 2.7  $\mu\text{m}$  spectral region

### **Figure 1**

## **1.2 Line parameters retrieval**

We used the multispectrum procedure developed at GSMA [13] to determine the line parameters. First, in order to minimize the effect of the apparatus function on the retrieved parameters, the experimental value of the Michelson's interferometer aperture was determined using spectra recorded at low pressures (not reported in the Table 1). The iris radius values of the FTS are indicated in Table 1. We did this verification even if the choice of the radius value is less critical than in the Doppler regime, since the H<sub>2</sub>O spectra were broadened by a pressure of CO<sub>2</sub> from 100Torr to 500Torr. The verification was done on several lines taken in the whole spectral region allowing a check of the nominal iris radius that can be used. No specific signature appeared on the residuals of the fit during this verification. The nominal iris

radius value was then used in the following analysis.

The multispectrum procedure enabled us to obtain simultaneously the position of the line, the line strength, the half-width and the line shift. An example of the multispectral fitting procedure is shown in Figure 2. The figure shows the simultaneous fit of three spectra with an absorption path length of 417,2 cm and different pressures (see table 1) in the upper panel and the residuals of the fit in the lower panel. Just over ten isolated lines were fit using two different values of self-broadening coefficients (broadening due to the pressure of H<sub>2</sub>O) in order to assess the impact of this parameter. A modification of 20 % of the fixed value of self-broadening coefficient does not change the retrieved CO<sub>2</sub>-broadening parameter. Therefore, the self-broadening coefficients were fixed to the values of the HITRAN2016 database edition [23]. The impact of the self-shift parameter was also negligible.

**Figure 2**

## 2. Theory

For the collision system under consideration, H<sub>2</sub>O-CO<sub>2</sub>, and temperatures of the study, quantum dynamical methods are too slow to be practical even if adequate potential energy surfaces were available. Thus, the calculations of the half-width and line shift for the H<sub>2</sub>O-CO<sub>2</sub> collision system were done using the semi-classical Modified Complex Robert-Bonamy formalism [24, 25] (MCRB). The half-width and the line shift are given by the real and imaginary parts, respectively, of the expression

$$(\gamma + i\delta)_{f \leftarrow i} = \frac{n_2}{2\pi c} \int_0^\infty v f(v) dv \int_0^\infty 2\pi b \left[ 1 - e^{-i\langle S_1 + \text{Im}(S_2) \rangle_{J_2}} e^{-\langle \text{Re}(S_2) \rangle_{J_2}} \right] db \quad (1).$$

In this expression,  $n_2$  is the number density of bath molecules,  $c$  is the speed of light,  $v$  is the

relative velocity,  $f(v)$  is the Maxwell-Boltzmann distribution of velocity,  $\langle \rangle_{J_2}$  is an average over the states of the bath molecules, and  $b$  is the impact parameter.  $S_1$ (imaginary) and  $S_2$ (complex) are the first and second order terms in the successive expansion of the Liouville scattering matrix, which depend on the ro-vibrational states in the optical transition, the associated collisionally induced jumps from these states, on the intermolecular potential, and the characteristics of the collision dynamics. Note, semi-classical refers to the fact that the internal structure of the colliding molecules is treated quantum mechanically and that the dynamics of the collision process are treated by classical mechanics. Thus, in an optical transition from  $f \leftarrow i$ , the active molecule will undergo collisions with the bath molecules, for which the trajectories are determined by classical mechanics. In these collisions, the initial and final states of the radiating molecule,  $i$  and  $f$ , will undergo collisionally induced transitions to states  $i'$  and  $f'$ , interrupting the radiation and causing collisional broadening and shifting. The states  $i'$  and  $f'$  are called *collisionally connected states* and are given by selection rules determined by the wavefunctions and intermolecular potential. Given the large number of terms in the intermolecular potential, there are many states,  $i'$  or  $f'$ , that are possible. The quantum mechanical components of the calculation are the energy of the states involved in the collisionally induced transitions and the wavefunctions for the states, which are used to determine reduced matrix elements (RME), which give the probability of a collisionally induced transition. A recent study [26] showed that MCRB calculations should use the ground state RMEs for all vibrational states.

The intermolecular potential used in the calculations was comprised of electrostatic terms, the induction and London dispersion terms, and an atom-atom component expanded to 20<sup>th</sup> order and rank 4. The atom-atom parameters were adjusted to bring the MCRB calculations in agreement with measurements of Tretyakov and Koshelev [27]. The final atom-atom parameters (called pot 23) are a change of  $\epsilon_{H-O}$ ,  $\epsilon_{H-C}$ ,  $\epsilon_{O-O}$ ,  $\epsilon_{O-C}$  by -30%, a change

of  $\sigma_{\text{H-O}}$  by -22.5% and a change of  $\sigma_{\text{H-C}}$ ,  $\sigma_{\text{O-O}}$ ,  $\sigma_{\text{O-C}}$  by -25% from the combination rule [28] values. All other parameters are the recommended values from the literature: The dipole moment of water and its vibrational dependence are taken from Shostak and Muentner [29]. The quadrupole moments come from Flygare and Benson [30]. The polarizability and its vibrational dependence are given by Luo *et al.* [31]. The ionization potential of water is taken from Ref. [32] and is a vibrationally-independent value. For CO<sub>2</sub>, the quadrupole moment is from the work of Graham *et al.* [33], the value of the polarizability is from Bogaard and Orr [34], and the ionization potential is from Tanaka *et al.* [35]. The numerical values are given in Refs. [36] and [11], for H<sub>2</sub>O and CO<sub>2</sub>, respectively.

The MCRB calculations included all real and imaginary components, atom-atom component expanded to high *order* and *rank*, trajectories determined solving Hamilton's equations, and explicit velocity averaging over the Boltzmann distribution.

### 3. MCRB calculations

Using HITRAN2016, all cold-band transitions for H<sub>2</sub><sup>16</sup>O, H<sub>2</sub><sup>18</sup>O, and H<sub>2</sub><sup>17</sup>O in the range 1300-5000 cm<sup>-1</sup> with  $J'' \leq 22$  and with full quantum assignments (note, in the UCL *ab initio* data [37] on HITRAN only J and symmetry are good quantum numbers, so some transitions do not have all quantum numbers.) were extracted. The number of lines in each cold band is listed in Table 2. The MCRB formalism includes the vibrational dependence of the line shape parameters, thus calculations were made for each band listed in Table 2. The calculations of the half-width and line shift were made at 13 temperatures from 200 to 3000 K in order to determine the temperature dependence of these parameters. For each band, the unique rotational transitions were determined for the three principal isotopologues; then calculations were made for the H<sub>2</sub><sup>16</sup>O isotopologue. These half-width and line shift values were used for the three isotopologues of this study since the line shape parameters are roughly

equal for all three. The last step was to use the line shape parameter data at the 13 temperatures to determine the temperature dependence by the Gamache-Vispoel model [38]. These data were used to create an improved line file for applications for water vapor in CO<sub>2</sub>-rich atmospheres. The previous H<sub>2</sub>O-CO<sub>2</sub> line file [17] neglects vibrational dependence for H<sub>2</sub><sup>16</sup>O, H<sub>2</sub><sup>18</sup>O, and H<sub>2</sub><sup>17</sup>O transitions and uses the rotation band half-widths for all transitions. The line shifts, due to their strong vibrational dependence, were from a semi-empirical algorithm [39] or from scaling.

## Table 2

### 4. Results and comparisons

#### 4.1 Spectral region around 6 μm

In this spectral region, line half-widths and shifts of H<sub>2</sub>O broadened by CO<sub>2</sub> were compared to previous laboratory measurements of Brown *et al.* [11] for the ν<sub>2</sub> fundamental band and to the MCRB calculations done here. The data sets are shown in Figs. 3 and 4 respectively for the half-widths and the pressure-induced line shift. In total 105 lines were analyzed. Shown in Fig. 3 are the measured half-widths with error bars (blue solid triangle symbols), the MCRB calculated half-widths shifted slightly to the left (black open diamond symbols), and the measured half-widths from Brown *et al.* [11] with error bars shifted slightly to the right (red open square symbols) versus wavenumber of the transition. Comparing the current measurements and calculations for 105 transitions gives an average percent difference (APD) of -2.9% and a standard deviation (SD) of 4.9%. Comparing our measurements with those of Brown *et al.* for 100 transitions gives an APD of -3.2% and a SD of 3.0%. Comparing the measurements of Brown *et al.* with our MCRB calculations for 100 transitions gives an APD of 0.17% and a SD of 5.5%. Thus, the half-width data of these two investigations and the calculations are in good agreement.

In Fig. 4, the measured line shifts with error bars (blue solid triangle symbols), the MCRB calculated line shifts shifted slightly to the left (black open diamond symbols), and the measured line shifts from Brown *et al.* [11] with error bars shifted slightly to the right (red open square symbols) are plotted versus wavenumber of the transition. A comparison of our measurements and calculations for 105 transitions shows an average deviation of  $-0.0043 \text{ cm}^{-1}\text{atm}^{-1}$  and a standard deviation of  $0.0048 \text{ cm}^{-1}\text{atm}^{-1}$ . Comparing our shift measurements with those of Brown *et al.* for 100 transitions gives an average deviation of  $-0.0035 \text{ cm}^{-1}\text{atm}^{-1}$  and a standard deviation of  $0.0029 \text{ cm}^{-1}\text{atm}^{-1}$ . Comparing the measurements of Brown *et al.* with our MCRB shift calculations for 100 transitions gives an average deviation of  $-0.00065 \text{ cm}^{-1}\text{atm}^{-1}$  and a standard deviation of  $0.0040 \text{ cm}^{-1}\text{atm}^{-1}$ . Again, showing excellent agreement between this study and that of Brown *et al.*

### Figure 3

### Figure 4

Brown *et al.* [8] presented Complex Robert-Bonamy calculations, which demonstrate that, when vibrational dependence is ignored, pairs of transitions with the same rotational quantum numbers interchanged have exactly the same half-width values and the line shifts have exactly the same magnitude with opposite signs. For asymmetric rotors, Brown *et al.* extended this property for pairs to an analysis on the parameters  $K_m$  and  $J_m$ , defined as the maximum values of  $K_a$  and  $J$ , respectively, in the transition quanta. Brown *et al.* also define  $\tau'$  and  $\tau''$  as  $\tau = K_a + K_c - J$  for use in their analysis. We observed similar behaviors as that seen in Table 8 of Brown *et al.* [11]. Examples are given in Table 3, where pair transitions are shown for the measured and calculated half-widths and line shifts. Table 3 shows that as a function of  $J_m$  and  $K_m$  the half-widths are nearly equal and the line shifts approximately equal but opposite in sign. A good example is the sequence for  $J_m = 4$  and  $K_m = 2$ . The exception is

when the line shift is very small, for which the measurements and calculations are difficult to make.

### Table 3

The good agreement with the previous measurements of Brown *et al.* [11] validates the choice of the experimental conditions for the measured spectra, as well as the intermolecular potential used in the MCRB calculations.

#### 4.2 Spectral region around 2.7 $\mu\text{m}$

As indicated in Table 1, for this spectral region, we recorded nine spectra with 2 different cells. We fitted simultaneously the spectra with the same cell length, it allows us to obtain lines parameters for transitions in a line intensity range from  $3.2 \times 10^{-22}$  to  $9.6 \times 10^{-20}$  cm/molec.: 60 transitions belong to the  $\nu_3$  band, 23 to the  $2\nu_2$  band and 15 to the  $\nu_1$  band. We did not find recent laboratory measurements for this spectral region in the literature. We compared our measurement and MCRB calculation results to the data from the Mars database [17]. Figure 5 shows the half-widths in  $\text{cm}^{-1} \text{atm}^{-1}$  from our measurements with error bars (blue solid triangle symbols), our MCRB calculations (black open diamond symbols), and the previous calculations of Gamache *et al.* [17] (red open square symbols) versus a line count. The data are arranged such that the first 16 points are  $\nu_1$  band data, points 17-40 are  $2\nu_2$  band data, and points 41-105 are  $\nu_3$  band data. The statistics for the agreement are given in top part of Table 4. The MCRB calculations made here include the vibrational dependence that was neglected in Ref. [17] and the intermolecular potential was optimized for the  $\text{H}_2\text{O}-\text{CO}_2$  collision system as discussed above. The result is that the calculations made here agree well with measurements with an APD of -1.1, -1.8, and -3.1 for the  $\nu_1$ ,  $2\nu_2$ , and  $\nu_3$  bands, respectively. The calculations that neglect the vibrational dependence have -13.8, -12.0, and -

11.8 APDs for the same data. The standard deviations show similar features. Given the relatively large value of the quadrupole moment of CO<sub>2</sub>, it could be argued that the vibrational dependence of the half-widths should not be too large. However, looking at the calculations to adjust the potential, the average difference between the potential used in Ref. [17] and the results from the final potential of this work (pot 23) is roughly 9%. This result suggests that the vibrational dependence for these bands is ~3-4%. We will study the vibrational dependence of the half-width in a future work.

#### Table 4

Figure 6 is a plot of the measured line shifts with error bars (blue solid triangle symbols), our MCRB calculations (black open diamond symbols), and the data of Gamache *et al.* [17]. Because the study of Gamache *et al.* [17] only made calculations for the rotation band, the values of the shifts in the database are from various approximate schemes from the work of Jacquemart *et al.* [39], or scaled directly from  $\delta_{\text{air}}$  from HITRAN2012 [40] ( $\delta_{\text{CO}_2} = \delta_{\text{air}} * 4.211$ ). In the plot, the red open star symbols correspond to Jacquemart *et al.*'s section 4.2.3 approximation; the red open circle symbols correspond to Jacquemart *et al.*'s section 4.1 approximation; the red open plus symbols correspond to Jacquemart *et al.*'s section 4.2.1 approximation; and the red asterisk symbols correspond to scaling the air-induced pressure shift. The statistics for the comparison of the line shifts are in the bottom part of Table 4. The average deviation between the measured and calculated line shifts goes between -0.001 to -0.004 cm<sup>-1</sup> atm<sup>-1</sup> with standard deviations around 0.006 cm<sup>-1</sup> atm<sup>-1</sup> for the 3 vibrational bands studied. The comparison with the approximate schemes used in Ref. [17] shows much larger average deviations, -0.07 to -0.08 cm<sup>-1</sup> atm<sup>-1</sup>, and standard deviations, ~0.065 cm<sup>-1</sup> atm<sup>-1</sup>. This figure and the statistics demonstrate the need for primary measurement or calculation to obtain good line shifts. It has been shown before [11, 41, 42] that scaling techniques lead to

very large errors, and it was stated [17] that the error from the semi-empirical line shift prediction routine can be large.

**Figure 5**

**Figure 6**

The line lists for the two previous spectral regions are given in the supplementary data.

### **4.3 Comparisons with data around 0.95 $\mu\text{m}$**

Borkov *et al.* [43] have measured the broadening and shift parameters of the water vapor spectral lines in the 10,100 - 10,800  $\text{cm}^{-1}$  region induced by pressure of carbon dioxide. We compared the measurements and calculations made here to their results for the half-width. Note, because the line shift is strongly dependent on vibration, a comparison of our line shifts to their data was not done. Borkov *et al.* made measurements for transitions in the  $\nu_1 + 2\nu_2 + \nu_3$ ,  $3\nu_1$ , and  $2\nu_1 + \nu_3$  bands. These data are compared with our measurements and calculations in the 2.7  $\mu\text{m}$  region ( $\nu_1$ ,  $2\nu_2$ , and  $\nu_3$  bands). Figure 7 shows the half-widths in  $\text{cm}^{-1} \text{atm}^{-1}$  for the our measurements with error bars (blue solid triangle, open triangle, and open diamond symbols for our  $\nu_1$ ,  $2\nu_2$ , and  $\nu_3$  band data, respectively), the MCRB calculations shifted slightly to the left (black solid star, open star, and star of David symbols for our  $\nu_1$ ,  $2\nu_2$ , and  $\nu_3$  band data, respectively), and the Borkov *et al.* data with error bars shifted slightly to the right (red solid circle, open circle, and open circle with a cross symbols for their  $\nu_1+2\nu_2+\nu_3$ ,  $\nu_1$ ,  $3\nu_1$ , and  $2\nu_1+\nu_3$  band data, respectively) versus line count. The data are arranged such that the first 13 points are  $\nu_1+2\nu_2+\nu_3$  band data, points 14-19 are  $3\nu_1$  band data, and points 20-45 are  $2\nu_1+\nu_3$  band data (labeled at the bottom of the figure). In total 45 transitions were compared between the data sets. The statistics for the comparison of our

measurements with the data of Borkov *et al.* are an APD of 1.5% with a SD of 7.3%; the comparison of our calculations to the data of Borkov *et al.* are an APD of -3.9% with a SD of 3.4%. The statistics imply a constant shift of our calculations, within 3-4%, from the Borkov *et al.* data. Even though the spectral regions of the two data sets are separated by about 6000  $\text{cm}^{-1}$ , there is good agreement among the data sets. This result implies the vibrational dependence is of order  $\sim 3\%$ , in agreement to the results from the previous section.

### Figure 7

## 5. Conclusion

New laboratory measurements of line-shape parameters of  $\text{H}_2\text{O}$  broadened by  $\text{CO}_2$  were performed. Two spectral regions were probed, i.e. 2.7 and 6  $\mu\text{m}$ , as they are of interest for the planetary atmospheres remote sensing. MCRB calculations of the half-width, line shift, and their temperature dependence were made for the cold bands of  $\text{H}_2\text{O}$  in the spectral range 1300-5000  $\text{cm}^{-1}$ . The results were compared with the literature values [11, 17, 43]. There is good agreement between the measured and calculated half-widths and line shifts with the data of Brown *et al.* in the 6  $\mu\text{m}$  region. In the 2.7  $\mu\text{m}$  region, our measurements and MCRB calculations agree well for both the half-widths and line shifts. Comparison with the half-widths and line shifts from Ref. [17] are not as good, showing the effects of neglecting vibrational dependence for the half-widths and using approximate prediction routines for the line shifts. Comparisons of our measured and calculated half-widths with the data of Borkov *et al.* [43] on the 0.9  $\mu\text{m}$  region show good agreement. The measurements are available as supplementary files. The calculations in the range 1300-5000  $\text{cm}^{-1}$  are available as a supplementary file. In the future, the MARS database [17] will be updated with the new parameters from this work and will be made publicly available, with a read\_me.txt file, as a file from one of the authors website ([faculty.uml.edu/robert\\_gamache](http://faculty.uml.edu/robert_gamache)). Note, using the

improved model of temperature dependence [38], the same database can be used for Mars, Venus, or any other planetary atmosphere rich in CO<sub>2</sub>.

### **Acknowledgements**

This work was supported by the Programme National de Planétologie (PNP) of CNRS-INSU co-funded by CNES. Several authors (RRG, BV) are pleased to acknowledge support of this research by the National Science Foundation through Grant No. AGS-1622676. Any opinions, findings, and conclusions or recommendations expressed in this material are those of the author(s) and do not necessarily reflect the views of the National Science Foundation. The authors sincerely thank Dr H. Tran from LMD (Paris) for many useful discussions, her expertise and advice on the line profile.

## Table captions

### Tables

- 1 Experimental conditions of recorded spectra with the Connes' type FTS ("DDM max" is the maximum of path difference for the interferogram measurement)
- 2 The Number of lines in each cold band from 1300 to 5000  $\text{cm}^{-1}$  for the three principal isotopologues of  $\text{H}_2\text{O}$
- 3 Example of measured  $\text{CO}_2$  broadened  $\text{H}_2\text{O}$  coefficients for "pair" transitions in the spectral region around 6  $\mu\text{m}$ .
- 4 Comparison of the measured half-widths and line shifts with the MCRB calculations of this work and with the calculations of Gamache *et al.* [17] in the spectral region around 2.7  $\mu\text{m}$ .. Given are the average percent difference (APD) and standard deviation (SD) in percent for the half-widths and the average deviation (Adev) and standard deviation in  $\text{cm}^{-1} \text{atm}^{-1}$  for the line shifts.

## Figure captions

Figure 1: Example of recorded spectra in the 2.7  $\mu\text{m}$  spectral region around  $3956\text{ cm}^{-1}$ , with an absorption path length of 817,8 cm (see table 1).

Figure 2: Example of the fit with the multispectrum procedure of a  $\text{H}_2\text{O}$  transition broadened by  $\text{CO}_2$  in the 2.7  $\mu\text{m}$  spectral region. The three spectra have an absorption path length of 417,2 cm (see table 1).

Figure 3:  $\text{CO}_2$ -broadened half-widths ( $\text{cm}^{-1}\text{ atm}^{-1}$ ) of  $\text{H}_2^{16}\text{O}$  transitions in the 6  $\mu\text{m}$  region versus wavenumber of the transition. Shown are measurements (Exp) done in this work (blue solid triangle symbols), MCRB calculations from this work (black open triangle symbols), and the measurements of Brown *et al.* [11] (red open square symbols). The error bars given for the measurements correspond to the  $2\sigma$  statistical uncertainty provided by the fit.

Figure 4:  $\text{CO}_2$  pressure-induced line shifts ( $\text{cm}^{-1}\text{ atm}^{-1}$ ) of  $\text{H}_2^{16}\text{O}$  transitions in the 6  $\mu\text{m}$  region versus wavenumber of the transition. Shown are measurements (Exp) from this work (blue solid triangle symbols), MCRB calculations from this work (black open triangle symbols), and the measurements of Brown *et al.* [11] (red open square symbols). The error bars given for the measurements correspond to the  $2\sigma$  statistical uncertainty provided by the fit.

Figure 5:  $\text{CO}_2$ -broadened half-widths ( $\text{cm}^{-1}\text{ atm}^{-1}$ ) of  $\text{H}_2^{16}\text{O}$  transitions in the 2.7  $\mu\text{m}$  region versus line count. For each vibrational band the points are ordered by the upper and lower state energy ordered index; index =  $J^*(J+1) + K_a - K_c + 1$ . Shown are measurements (Exp) from this work (blue solid triangle symbols), MCRB calculations from this work (black open diamond symbols), and the previous calculations of Gamache *et al.* [17] (red open square symbols). The data are

arranged such that the first 16 points are  $\nu_1$  band data, points 17-40 are  $2\nu_2$  band data, and points 41-105 are  $\nu_3$  band data. The error bars given for the measurements correspond to the  $2\sigma$  statistical uncertainty provided by the fit.

Figure 6:  $\text{CO}_2$  pressure-induced line shifts ( $\text{cm}^{-1} \text{ atm}^{-1}$ ) of  $\text{H}_2^{16}\text{O}$  transitions in the  $2.7 \mu\text{m}$  region versus line count. For each vibrational band the points are ordered by the upper and lower state energy ordered index;  $\text{index} = J^*(J+1) + K_a - K_c + 1$ . Shown are measurements (Exp) from this work (blue solid triangle symbols), MCRB calculations from this work (black open diamond symbols), from Gamache *et al.* [17]; the red open star symbols correspond to Jacquemart *et al.*'s [39] section 4.2.3 approximation; the red open circle symbols correspond to Jacquemart *et al.*'s section 4.1 approximation; the red open plus symbols correspond to Jacquemart *et al.*'s section 4.2.1 approximation; and the red asterisk symbols correspond to scaling the air-induced pressure shift. See text for details. The data are arranged such that the first 16 points are  $\nu_1$  band data, points 17-40 are  $2\nu_2$  band data, and points 41-105 are  $\nu_3$  band data. The error bars given for the measurements correspond to the  $2\sigma$  statistical uncertainty provided by the fit.

Figure 7: Comparison of the half-widths ( $\text{cm}^{-1} \text{ atm}^{-1}$ ) from the measurements (Exp) blue solid triangle, open triangle, and open diamond symbols for our  $\nu_1$ ,  $2\nu_2$ , and  $\nu_3$  band data, respectively), the MCRB calculations (black solid star, open star, and star of David symbols for our  $\nu_1$ ,  $2\nu_2$ , and  $\nu_3$  band data, respectively), and the Borkov *et al.* [43] data (red solid circle, open circle, and open circle with a cross symbols for our  $\nu_1$ ,  $2\nu_2$ , and  $\nu_3$  band data, respectively) versus line count. The data are arranged such that the first 13 points are  $\nu_1+2\nu_2+\nu_3$  band data, points 14-19 are  $3\nu_1$  band data, and points 20-45 are  $2\nu_1+\nu_3$  band data. For each vibrational band

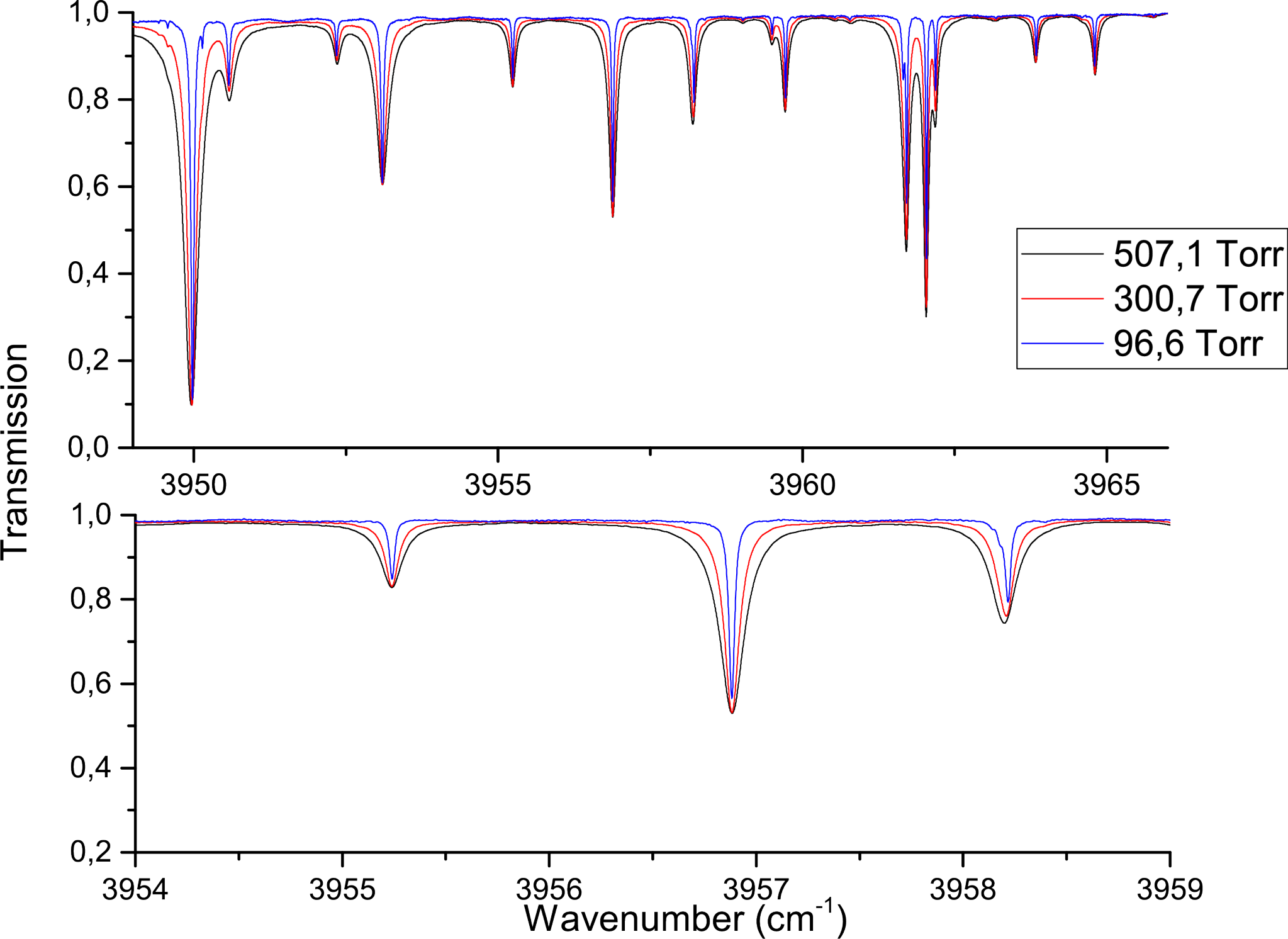
the points are ordered by the upper and lower state energy ordered index; index =  $J*(J+1) + K_a - K_c + 1$ . The error bars given for the measurements correspond to the  $2\sigma$  statistical uncertainty provided by the fit.

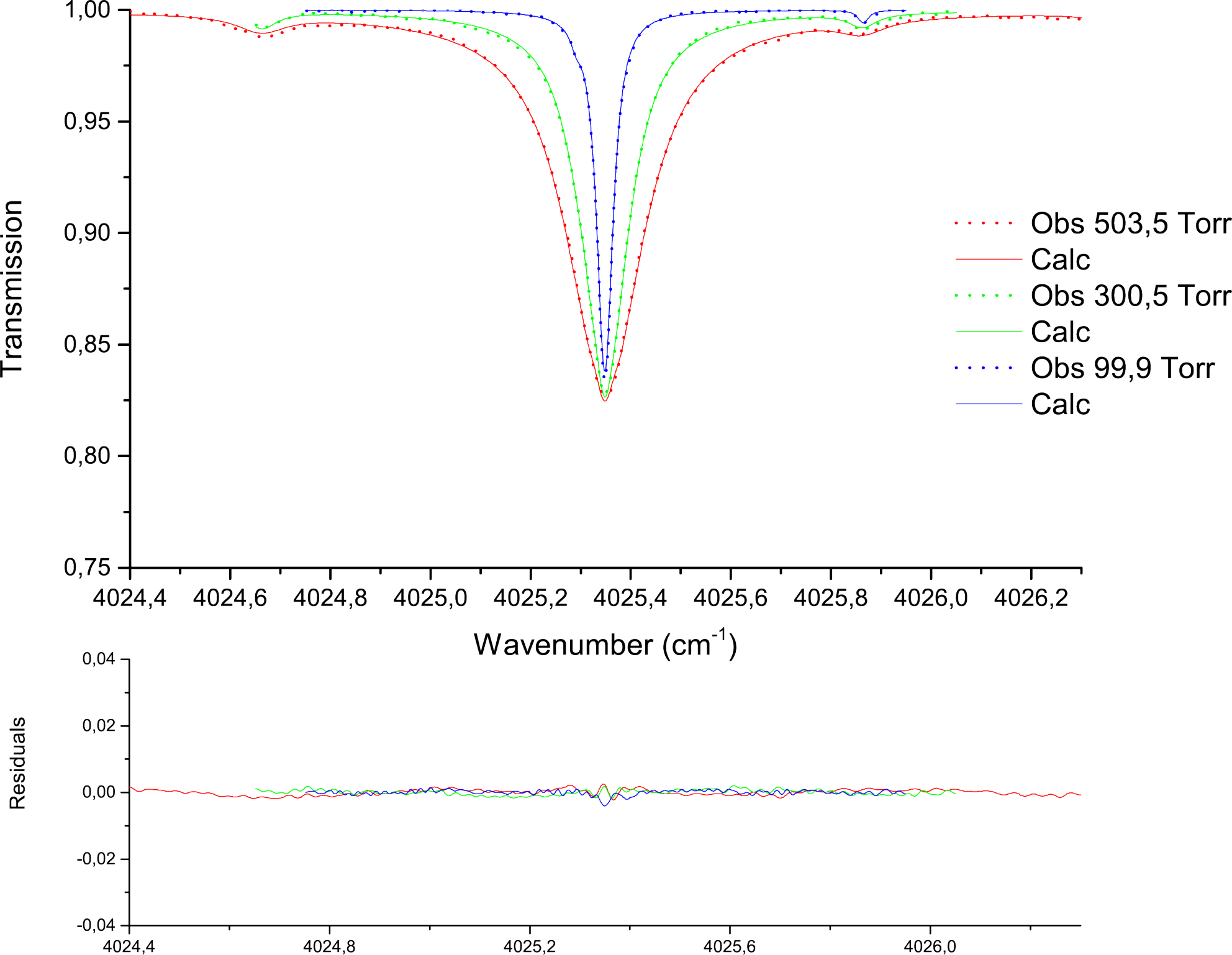
## References

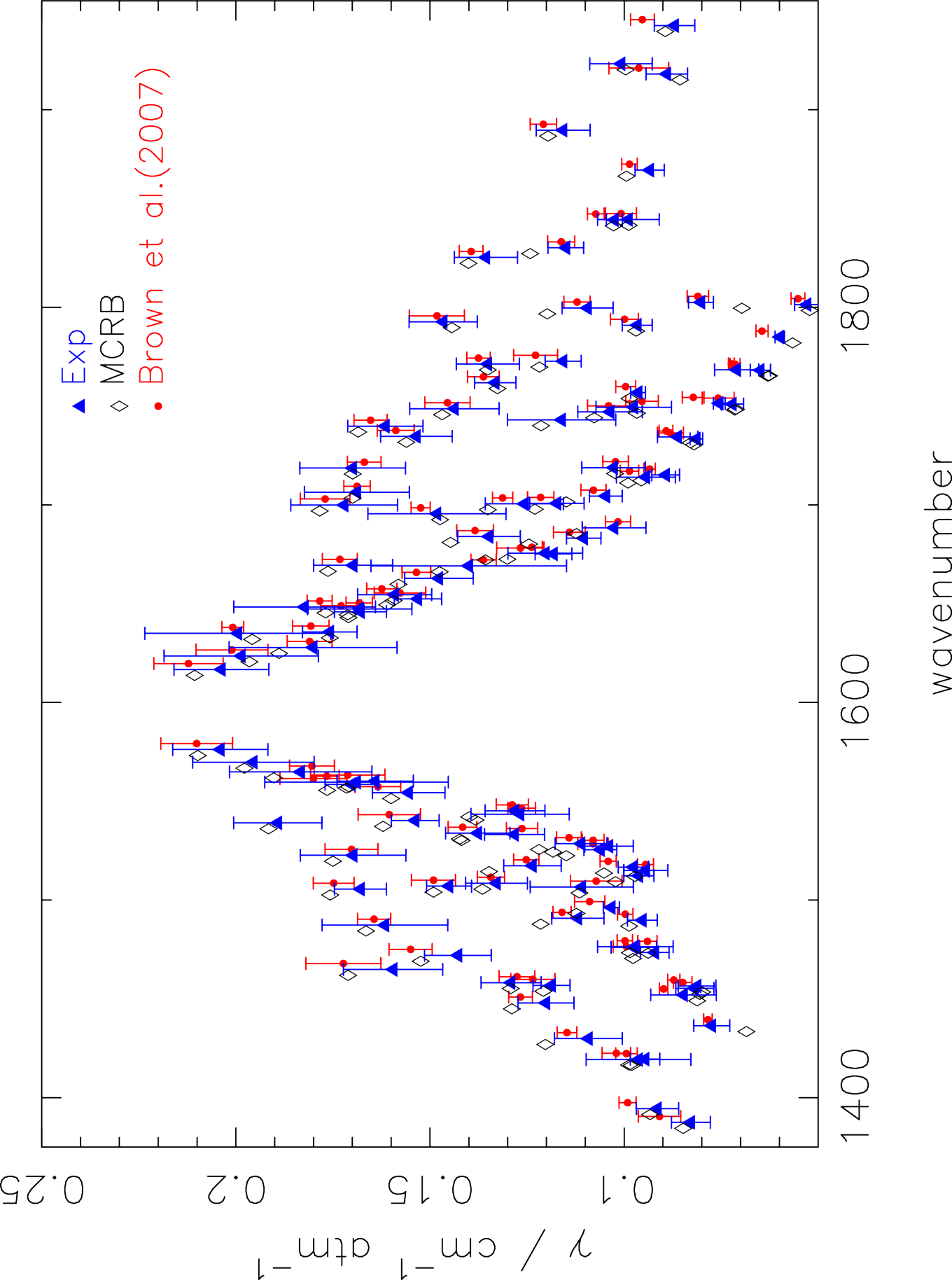
- [1] de Bergh C. Isotopic Ratios in Planetary Atmospheres, *Adv. Space Res.* 1995; **15**: 427-40.
- [2] Owen T, Maillard JP, de Bergh C, B.L. Lutz. Deuterium on Mars: the abundance of HDO and the value of D/H, *Science* 1988; **240**: 1767-70.
- [3] Carr MH. D/H on Mars: effects of floods, volcanism, impacts, and polar processes, *Icarus* 1990; **87**: 210-27.
- [4] Encrenaz T, Lellouch E, Paubert G, Gulkis S. The water vapor vertical distribution on mars from millimeter transitions of HDO and  $\text{H}_2^{18}\text{O}$ , *Planet. Space Sci.* 2001; **49**: 731-41.
- [5] Encrenaz T, Bézard B, Owen T, Lebonnois S, Lefèvre F, Greathouse T, Richter M, Lacyg J, Atreyah S, Wongh AS, Forget F. Infrared imaging spectroscopy of Mars:  $\text{H}_2\text{O}$  mapping and determination of  $\text{CO}_2$  isotopic ratios, *Icarus* 2005; **179**: 43-54.
- [6] Bertaux JL, Vandaele AC, Korablev O, Villard E, Fedorova A, Fussen D, Quémerais E, Belyaev D, Mahieux A, Montmessin F, Muller C, Neefs E, Nevejans D, Wilquet V, Dubois JP, Hauchecorne A, Stepanov A, Vinogradov I, Rodin A. A warm layer in Venus' cryosphere and high-altitude measurements of HF, HCl,  $\text{H}_2\text{O}$  and HDO, *Nature* 2007; **450**: 646-9.
- [7] Fedorova A, Korablev O, Vandaele A-C, Bertaux J-L, Belyaev D, Mahieux A, Neefs E, Wilquet WV, Drummond R, Montmessin F, Villard E. HDO and  $\text{H}_2\text{O}$  vertical distributions and isotopic ratio in the Venus mesosphere by Solar Occultation at Infrared spectrometer on board Venus Express, *J. Geophys. Res.* 2008; **113**: E00B22.
- [8] Villanueva GL, Mumma MJ, Novak RE, Käufel HU, Hartogh P, Encrenaz T, Tokunaga A, Khayat A, Smith MD. Strong water isotopic anomalies in the martian atmosphere: Probing current and ancient reservoirs, *Science* 2015; **348**: 218-21.
- [9] Good SP, Noone D, Kurita N, Benetti M, Bowen GJ. D/H isotope ratios in the global hydrologic cycle, *Geophysical Research Letters* 2015; **42**: 5042-50.
- [10] Yang L, Ciesla FJ, Alexander CMOD. The D/H ratio of water in the solar nebula during its formation and evolution, *Icarus* 2013; **226**: 256-67.
- [11] Brown LR, Humphrey CM, Gamache RR.  $\text{CO}_2$ -broadened water in the pure rotation and  $\nu_2$  fundamental regions, *J. Mol. Spectrosc.* 2007; **246**: 1-21.
- [12] Gamache RR, Neshyba SP, Plateaux JJ, Barbe A, Régalia L, Pollack JB.  $\text{CO}_2$ -Broadening of Water-Vapor Lines, *J. Mol. Spectrosc.* 1995; **170**: 131-51.
- [13] Plateaux JJ, Regalia L, Boussin C, Barbe A. Multispectrum fitting technique for data recorded by Fourier transform spectrometer: application to  $\text{N}_2\text{O}$  and  $\text{CH}_3\text{D}$ , *Journal of Quantitative Spectroscopy and Radiative Transfer* 2001; **68**: 507-20.
- [14] Devi VM, Benner DC, Sung K, Crawford TJ, Gamache RR, Renaud CL, Smith MAH, Mantz AW, Villanueva GL. Line parameters for  $\text{CO}_2$  broadening in the  $\nu_2$  band of  $\text{HD}^{16}\text{O}$ , *Journal of Quantitative Spectroscopy and Radiative Transfer* 2017; **187**: 472-88.
- [15] Devi VM, Benner DC, Sung K, Crawford TJ, Gamache RR, Renaud CL, Smith MAH, Mantz AW, Villanueva GL. Line parameters for  $\text{CO}_2$ - and self-broadening in the  $\nu_3$  band of  $\text{HD}^{16}\text{O}$ , *Journal of Quantitative Spectroscopy and Radiative Transfer* 2017; **203**: 158-74.
- [16] Devi VM, Benner DC, Sung K, Crawford TJ, Gamache RR, Renaud CL, Smith MAH, Mantz AW, Villanueva GL. Line parameters for  $\text{CO}_2$ - and self-broadening in the  $\nu_1$  band of  $\text{HD}^{16}\text{O}$ , *Journal of Quantitative Spectroscopy and Radiative Transfer* 2017; **203**: 133-57.

- [17] Gamache RR, Faresse M, Renaud CL. A spectral line list for water isotopologues in the 1100–4100  $\text{cm}^{-1}$  region for application to  $\text{CO}_2$ -rich planetary atmospheres, *Journal of Molecular Spectroscopy* 2016; **326**: 144-50.
- [18] Connes P, Michel G. Astronomical Fourier spectrometer, *Applied Optics* 1975; **14**: 2067-84.
- [19] Plateaux JJ, Barbe A, Delahaigue A. Reims high resolution Fourier transform spectrometer. Data reduction for ozone, *Spectrochimica Acta Part A: Molecular and Biomolecular Spectroscopy* 1995; **51**: 1153-69.
- [20] Régalia L, Oudot C, Thomas X, Von der Heyden P, Decatoire D. FTS improvements and connection with a long White cell. Application:  $\text{H}_2\text{O}$  intensity measurements around  $1200\text{cm}^{-1}$ , *Journal of Quantitative Spectroscopy and Radiative Transfer* 2010; **111**: 826-42.
- [21] White JU. Long optical paths of large aperture, *Journal of the Optical Society of America* 1942; **32**: 285-8.
- [22] Loos J, Birk M, Wagner G. Measurement of positions, intensities and self-broadening line shape parameters of  $\text{H}_2\text{O}$  lines in the spectral ranges  $1850\text{--}2280\text{cm}^{-1}$  and  $2390\text{--}4000\text{cm}^{-1}$ , *Journal of Quantitative Spectroscopy and Radiative Transfer* 2017; **203**: 119-32.
- [23] Gordon IE, Rothman LS, Hill C, R.V.Kochanov, Tan Y, Bernath PF, Birk M, Boudon V, Campargue A, Chance KV, Drouin BJ, Flaud J-M, Gamache RR, Jacquemart D, Perevalov VI, Perrin A, Smith M-AH, Tennyson J, Tran H, Tyuterev VG, Toon GC, Hodges JT, Shine KP, Barbe A, Csaszar A, Devi MV, Furtenbacher T, Harrison JJ, Jolly A, Johnson T, Karman T, Kleiner I, Kyuberis A, Loos J, Lyulin O, Mikhailenko SN, Moazzen-Ahmadi N, Müller HSP, Naumenko O, Nikitin A, Polyansky O, Rey M, Rotger M, Sharpe S, Sung K, Starikova E, Tashkun SA, Auwera JV, Wagner G, Wilzewski J, Wcisło P, Yu S, Zak E. The HITRAN2016 Molecular Spectroscopic Database, *Journal of Quantitative Spectroscopy and Radiative Transfer* 2017; **203**: 3-69.
- [24] Robert D, Bonamy J. Short range force effects in semiclassical molecular line broadening calculations, *J. Phys. France* 1979; **40**: 923-43.
- [25] Ma Q, Tipping RH, Boulet C. Modification of the Robert-Bonamy formalism in calculating Lorentzian half-widths and shifts, *J. Quant. Spectrosc. Radiat. Transfer* 2007; **103**: 588-96.
- [26] Gamache RR, Vispoel B, Renaud CL, Cleghorn K, Hartmann L. Vibrational dependence, temperature dependence, and prediction of line shape parameters for the  $\text{H}_2\text{O}\text{-H}_2$  collision system, *Icarus* 2019; **326**: 186-96.
- [27] Tretyakov MY, Koshelev MA. private communication, 2018.
- [28] Hirschfelder JO, Curtiss CF, Bird RB. *Molecular Theory of Gases and Liquids*, Wiley, New York 1964.
- [29] Shostak SL, Muentner JS. The dipole moment of water.II. Analysis of the vibrational dependence of the dipole moment in terms of a dipole moment function, *J. Chem. Phys.* 1991; **94**: 5883-90.
- [30] Flygare WH, Benson RC. The Molecular Zeeman Effect in Diamagnetic molecules and the determination of molecular magnetic moments ( $g$  values), magnetic susceptibilities, and molecular quadrupole moments, *Mol. Phys.* 1971; **20**: 225-50.
- [31] Luo Y, Agren H, Vahtras O, Jorgensen P, Spirko V, Hetttema H. Frequency-dependent polarizabilities and first hyperpolarizabilities of  $\text{H}_2\text{O}$ , *J. Chem. Phys.* 1993; **98**: 7159-64.
- [32] Lide DR, Editor, *CRC Handbook of Physics and Chemistry*. 92<sup>nd</sup> ed., 2011, The Chemical Rubber Company: Cleveland, OH.

- [33] Graham C, Pierrus J, Raab RE. Measurements of the electric quadrupole moments of CO<sub>2</sub>, CO and N<sub>2</sub>, *Mol. Phys.* 1989; **67**: 939-55.
- [34] Bogaard MP, Orr BJ. In: A.D. Buckingham, Editor, *MPT International Review of Science, Physical Chemistry, Series Two, Vol. 2. Molecular Structure and Properties*, Butterworths, London (Chapter 5) 1975.
- [35] Tanaka Y, Jursa AS, LeBlanc FJ. Higher Ionization Potentials of Linear Triatomic Molecules. I. CO<sub>2</sub>, *J. Chem. Phys.* 1960; **32**: 1199-205.
- [36] Gamache RR, Lynch R, Plateaux JJ, Barbe A. Halfwidths and Line Shifts of Water Vapor Broadened by CO<sub>2</sub>: Measurements and Complex Robert-Bonamy Formalism Calculations, *J. Quant. Spectrosc. Radiat. Transfer* 1997; **57**: 485-96.
- [37] Barber RJ, Tennyson J, Harris GJ, Tolchenov RN. A high-accuracy computed water line list, *Mon. Not. R. Astron. Soc.* 2006; **368**: 1087-94.
- [38] Gamache RR, Vispoel B. On the temperature dependence of half-widths and line shifts for molecular transitions in the microwave and infrared regions, *J. Quant Spectrosc. Radiat. Transfer* 2018; **217**: 440-52.
- [39] Jacquemart D, Gamache R, Rothman LS. Semi-empirical calculation of air-broadened half-widths and air pressure-induced frequency shifts of water-vapor absorption lines, *J. Quant. Spectrosc. Radiat. Transfer* 2005; **96**: 205-39.
- [40] Rothman LS, Gordon IE, Babikov Y, Barbe A, Chris Benner D, Bernath PF, Birk M, Bizzocchi L, Boudon V, Brown LR, Campargue A, Chance K, Cohen EA, Coudert LH, Devi VM, Drouin BJ, Fayt A, Flaud JM, Gamache RR, Harrison JJ, Hartmann JM, Hill C, Hodges JT, Jacquemart D, Jolly A, Lamouroux J, Le Roy RJ, Li G, Long DA, Lyulin OM, Mackie CJ, Massie ST, Mikhailenko S, Müller HSP, Naumenko OV, Nikitin AV, Orphal J, Perevalov V, Perrin A, Polovtseva ER, Richard C, Smith MAH, Starikova E, Sung K, Tashkun S, Tennyson J, Toon GC, Tyuterev VG, Wagner G. The HITRAN2012 molecular spectroscopic database, *Journal of Quantitative Spectroscopy and Radiative Transfer* 2013; **130**: 4-50.
- [41] Gamache RR, Laraia AL, Lamouroux J. Half-widths, their temperature dependence, and line shifts for the HDO-CO<sub>2</sub> system for applications to planetary atmospheres, *Icarus* 2011; **213**: 720-30.
- [42] Vispoel B, Fissiaux L, Lepère M. CO<sub>2</sub>-broadening coefficients in the  $\nu_3$  fundamental band of methane, *Journal of Molecular Spectroscopy* 2019.
- [43] Borkov YG, Petrova TM, Solodov AM, Solodov AA. Measurements of the broadening and shift parameters of the water vapor spectral lines in the 10,100–10,800 cm<sup>-1</sup> region induced by pressure of carbon dioxide, *Journal of Molecular Spectroscopy* 2018; **344**: 39-45.







Exp  
MCRB  
Brown(2007)

0.05

$\delta / \text{cm}^{-1} \text{atm}^{-1}$

0

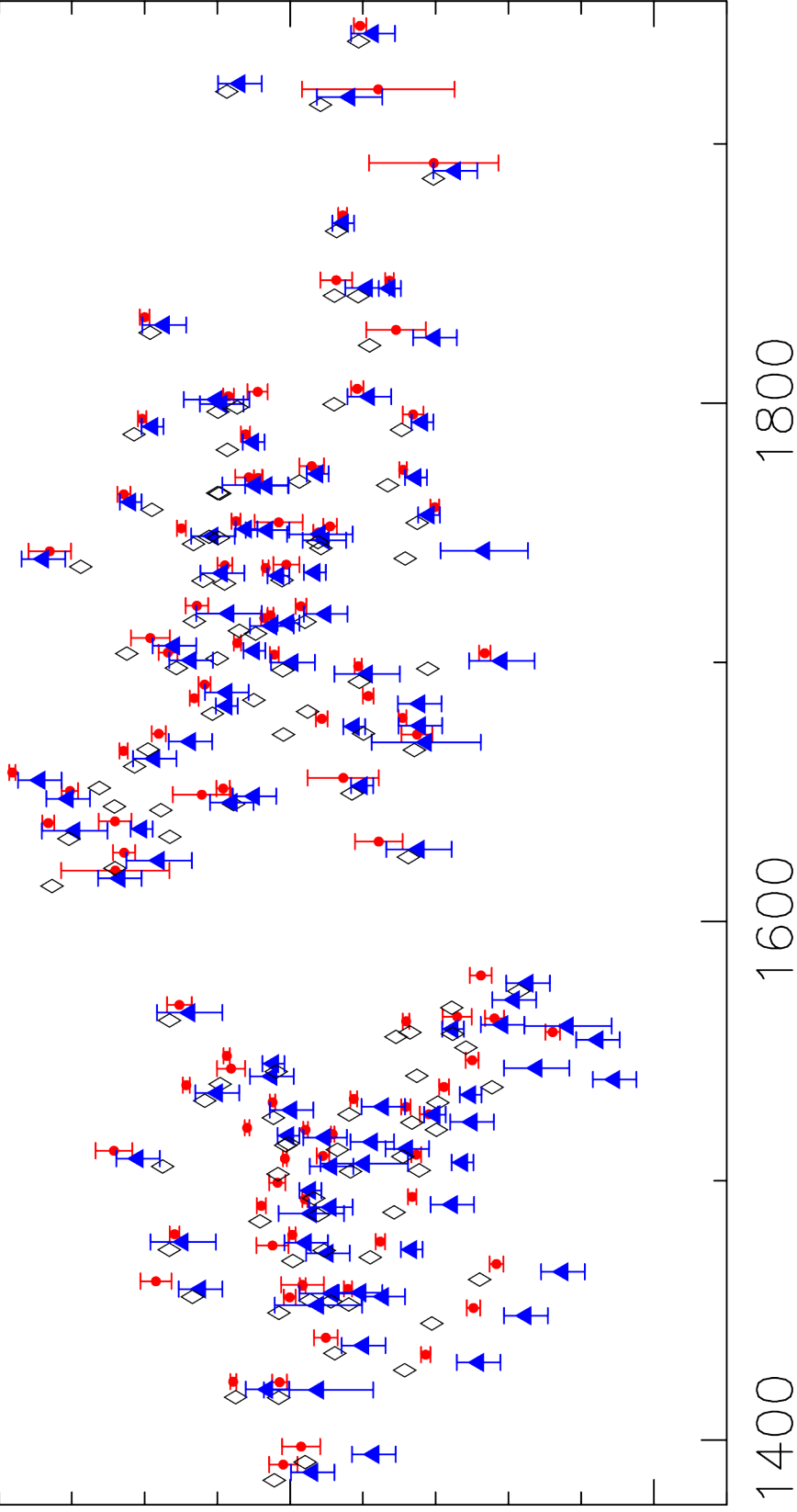
-0.05

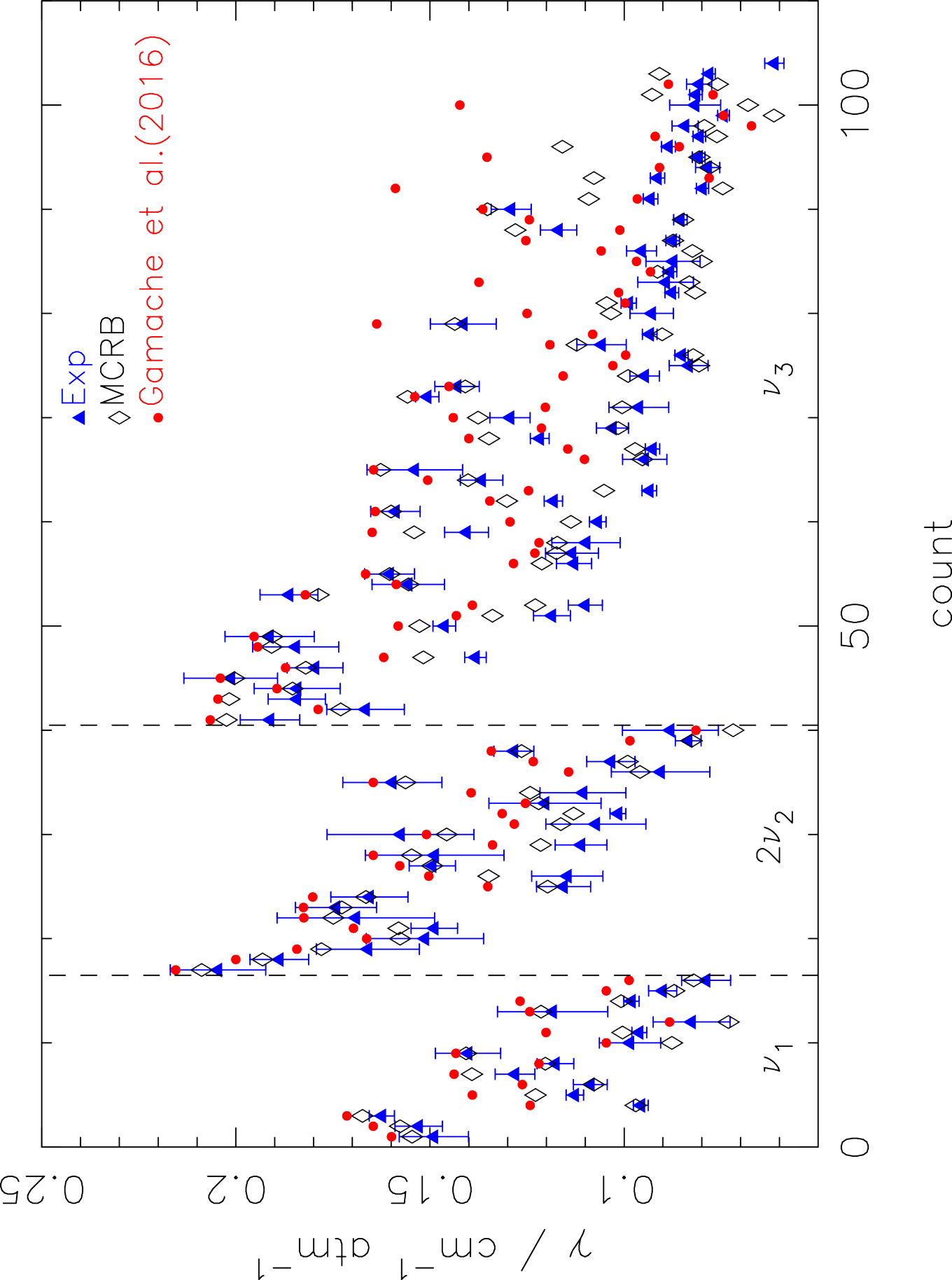
1400

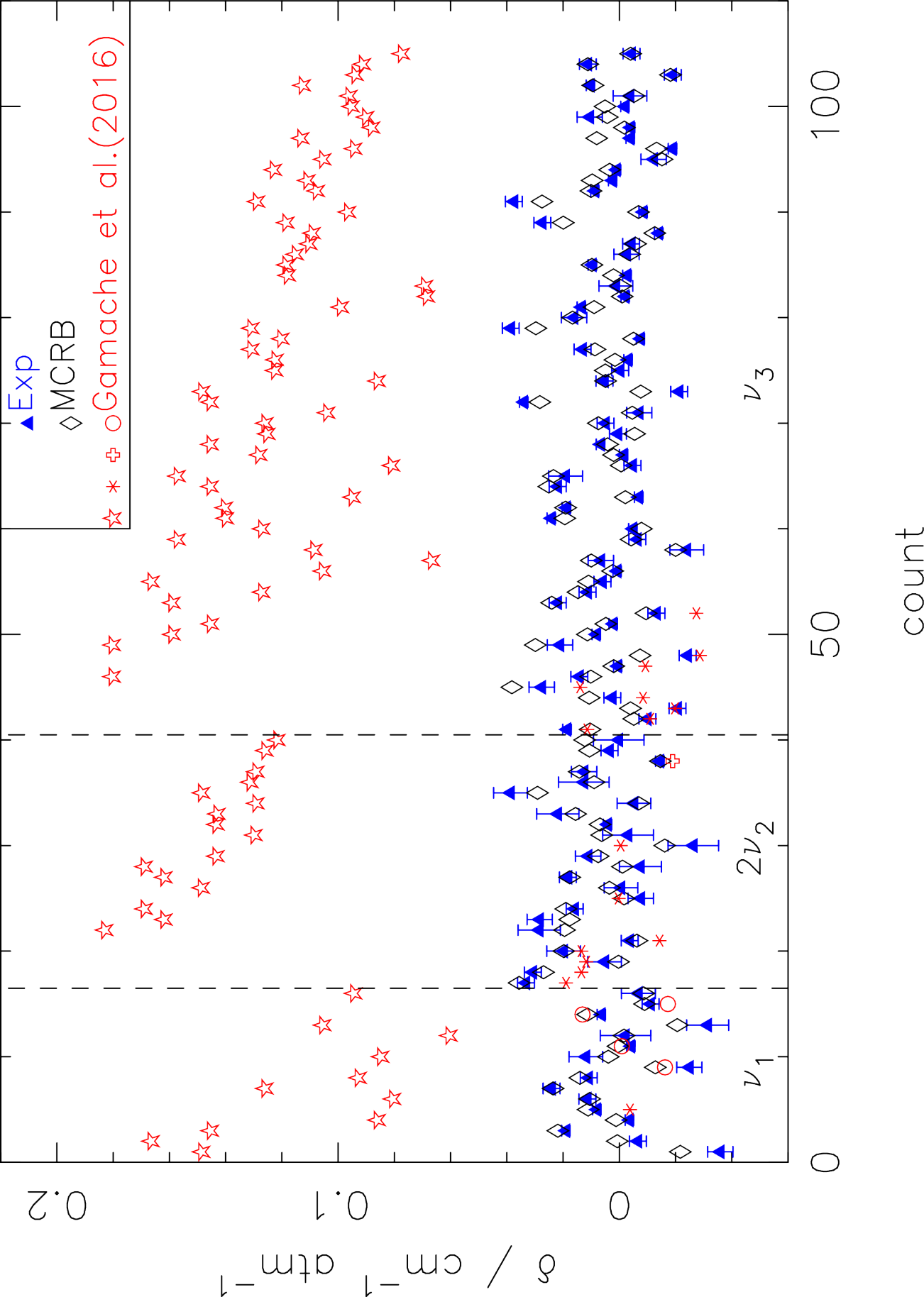
1600

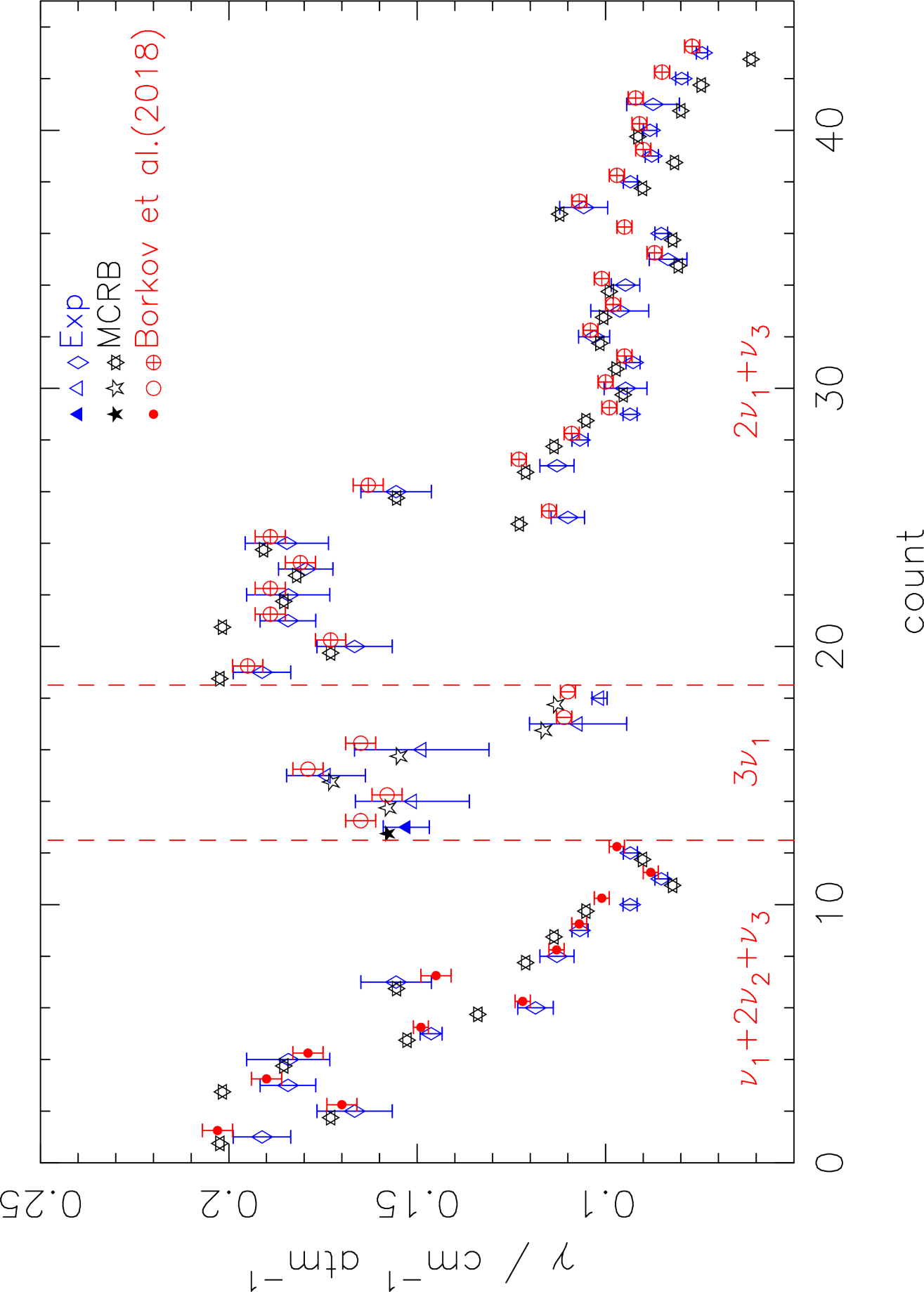
1800

wavenumber









Spectral region 2.7 $\mu\text{m}$		iris radius (aperture)= 2,25 mm			
Cell length (cm)	DDM max (cm)	Total Pressure in Torr	P(H <sub>2</sub> O) in Torr	P(CO <sub>2</sub> ) in Torr	Temperature in Kelvin
13.6	46	504.2	2.05	502.2	295.5
	61	300.9	1.22	299.7	295.5
	88	99.3	0.40	98.9	295.6
417.2	35	503.5	2.03	501.5	292.7
	41	300.5	1.21	299.3	292.9
	59	99.9	0.40	99.5	293.2
817.8	29	507.1	2.10	505.0	293.3
	33	300.7	1.24	299.4	293.4
	59	96.6	0.40	96.2	293.3

Spectral region 6 $\mu\text{m}$		iris radius (aperture)= 2,5 mm			
Cell length (cm)	DDM max (cm)	Total Pressure in Torr	P(H <sub>2</sub> O) in Torr	P(CO <sub>2</sub> ) in Torr	Temperature in Kelvin
13.6	46	502.9	2.07	500.8	295.4
	69	298.3	1.23	297.1	295.4
	70	100.3	0.41	99.9	295.5

**Table 1**

Band	H <sub>2</sub> <sup>16</sup> O	H <sub>2</sub> <sup>18</sup> O	H <sub>2</sub> <sup>17</sup> O
0 0 0 ← 0 0 0	112	7	0
0 1 0 ← 0 0 0	2326	1297	915
0 2 0 ← 0 0 0	2150	971	493
1 0 0 ← 0 0 0	2479	1320	781
0 0 1 ← 0 0 0	2950	1593	1096
0 1 1 ← 0 0 0	424	165	94
0 3 0 ← 0 0 0	783	368	86
1 1 0 ← 0 0 0	383	163	57
total	11607	5884	3522

**Table 2**

Rotational Assignment	Jm	Km	$\tau'$	$\tau''$	$\gamma_{\text{Exp.}}$ cm <sup>-1</sup> /atm	$\gamma_{\text{MCRB}}$ cm <sup>-1</sup> /atm	$\delta_{\text{Exp.}}$ cm <sup>-1</sup> /atm	$\delta_{\text{MCRB}}$ cm <sup>-1</sup> /atm
1 1 0 ← 1 0 1	1	1	0	0	0.2037	0.2106	0.02340	0.03271
1 0 1 ← 1 1 0	1	1	0	0	0.2040	0.2098	-0.03270	-0.03144
4 4 0 ← 3 3 1	4	4	0	1	0.0989	0.0988	-0.01060	-0.00610
3 3 1 ← 4 4 0	4	4	1	0	0.0963	0.0980	-0.00393	0.00157
4 4 1 ← 3 3 0	4	4	1	0	0.1025	0.1027	-0.01370	-0.00934
3 3 0 ← 4 4 1	4	4	0	1	0.0946	0.0987	0.00312	0.00747
4 3 1 ← 3 2 2	4	3	0	1	0.1094	0.1198	0.00948	0.00990
3 2 2 ← 4 3 1	4	3	1	0	0.1092	0.1203	-0.02590	-0.01575
4 2 2 ← 4 1 3	4	2	0	0	0.1681	0.1712	0.03050	0.02413
4 1 3 ← 4 2 2	4	2	0	0	0.1689	0.1715	-0.03820	-0.02234
3 1 2 ← 4 2 3	4	2	0	0	0.1428	0.1524	-0.00528	-0.00038
4 2 3 ← 3 1 2	4	2	0	0	0.1535	0.1561	-0.00341	0.00110
4 2 3 ← 4 1 4	4	2	0	0	0.1104	0.1245	0.00870	0.01069
4 1 4 ← 4 2 3	4	2	0	0		0.1265		-0.01342
3 2 1 ← 2 1 2	3	2	0	1	0.1615	0.1685	0.03390	0.02876
2 1 2 ← 3 2 1	3	2	1	0	0.1595	0.1711	-0.03750	-0.02604
4 0 4 ← 3 1 3	4	1	0	1	0.1182	0.1357	-0.00883	0.00092
3 1 3 ← 4 0 4	4	1	1	0	0.1236	0.1348	0.00028	0.00026
3 2 1 ← 3 1 2	3	2	0	0	0.1679	0.1710	0.00803	0.01775
3 1 2 ← 3 2 1	3	2	0	0	0.1641	0.1708	-0.02920	-0.01647
2 0 2 ← 1 1 1	2	1	0	1	0.1801	0.1889	-0.01770	-0.01626
1 1 1 ← 2 0 2	2	1	1	0	0.1833	0.1902	0.01380	0.01658
6 2 5 ← 5 1 4	6	2	1	0	0.1332	0.1326	0.02190	0.01900
5 1 4 ← 6 2 5	6	2	0	1	0.1201	0.1289	-0.03240	-0.01947
7 1 7 ← 6 0 6	7	1	1	0	0.0862	0.0829	0.00939	0.01197
6 0 6 ← 7 1 7	7	1	0	1	0.0818	0.0805	-0.01280	-0.00807
7 0 7 ← 6 1 6	7	1	0	1	0.0814	0.0820	0.00160	0.00900
6 1 6 ← 7 0 7	7	1	1	0	0.0812	0.0799	-0.00583	-0.00562
8 1 8 ← 7 0 7	8	1	1	0	0.0755	0.0712	0.00601	0.01111

707 ← 818	8	1	0	1	0.0774	0.0685	-0.01010	-0.00614
-----------	---	---	---	---	--------	--------	----------	----------

**Table 3**

	Band	1 0 0 ← 0 0 0	0 2 0 ← 0 0 0	0 0 1 ← 0 0 0
	# points	16	24	66
Half-width				
Exp-MCRB	APD	-1.1	-1.8	-3.1
	SD	5.7	4.9	6.0
Exp-Gamache et al.[32]	APD	-13.8	-12.0	-11.8
	SD	9.7	8.5	9.4
Line shift				
Exp-MCRB	Adev <sup>†</sup>	-0.0037	-0.0014	-0.0025
	SD <sup>†</sup>	0.0056	0.0062	0.0060
Exp-Gamache et al.[32]	Adev <sup>†</sup>	-0.0750	-0.0666	-0.0848
	SD <sup>†</sup>	0.0623	0.0683	0.0664

<sup>†</sup> in units of  $\text{cm}^{-1} \text{atm}^{-1}$

**Table 4**